iScience

Article

Analysis of anion exchange membrane water electrolyzer performance and its evolution over time

Graphical abstract

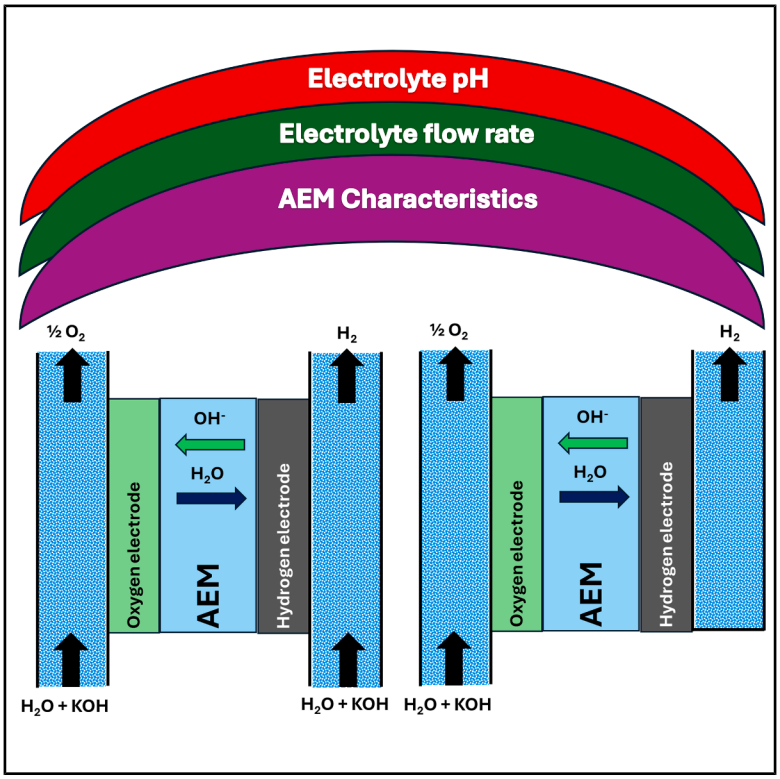

Highlights

- Investigate the MEA activation process
- Demonstrate electrolyte flow rate effects, advantages of dry vs. wet cathode
- Investigate the impact of film drying on AEM characteristics and performance
- Demonstrate the importance of supporting electrolyte pH changes during operation

Authors

Noor Ul Hassan, Radhika Iyer, Andrew Boudreau, ..., Scott Mauger, Bryan S. Pivovar, Shaun M. Alia

Correspondence

shaun.alia@nrel.gov

In brief

Electrochemistry; Energy storage; Energy Systems

Ul Hassan et al., 2025, iScience *28*, 114037
December 19, 2025
https://doi.org/10.1016/j.isci.2025.114037

CellPress

iScience

CellPress
OPEN ACCESS

Article

Analysis of anion exchange membrane water electrolyzer performance and its evolution over time

Noor Ul Hassan,[1] Radhika Iyer,[1] Andrew Boudreau,[1] Alexis Palau,[1] Chance Parrish,[1] Scott Mauger,[1] Bryan S. Pivovar,[1] and Shaun M. Alia[1,2,*]

[1]Chemistry and Nanoscience Center, National Renewable Energy Laboratory, Golden, CO 80401, USA

[2]Lead contact

*Correspondence: shaun.alia@nrel.gov

https://doi.org/10.1016/j.isci.2025.114037

SUMMARY

Understanding water, evolved gas, and ionic transport in membrane-electrode-assemblies (MEAs) is essential for the development of high performance and durable anion exchange membrane water electrolyzers (AEMWEs). This study evaluates the MEA conditioning process, operating conditions, and short-term stability in a 1 M potassium hydroxide (KOH) electrolyte, focusing on the underlying transport phenomena. We observe a significant initial voltage loss in continuous cell operation, which could be associated with gas bubble accumulation, transport layer or flow field passivation, and changes in the catalyst oxidation state. Further, we investigate the effects of materials and operational configurations, including the membrane type and thickness, and the electrolyte flow rate, including KOH being fed to both electrodes as well as to the anode only. Furthermore, the effect of membrane drying temperature on *ex situ* as well as *in situ* electrochemical performance is evaluated. Finally, we discuss 700 h of AEMWE operation at 1 A/cm^2, highlighting the underlying degradation phenomena.

INTRODUCTION

The use of renewable energy sources such as solar, wind, and tidal hydraulics has tremendously increased due to their gradual cost reduction.[1,2] However, the intermittent nature of such renewable energy sources requires large-scale storage solutions to allow for continued market penetration.[3] Hydrogen is attractive in energy storage due to its high energy density, the ability to store in large amounts for short as well as long durations, and the ability to convert between chemical and electrical forms of energy.[4]

Hydrogen production by low temperature water electrolysis is a well-established technology. Among low-temperature electrolysis systems (<100°C), the alkaline water electrolyzer (AWE) is well-known and has been commercially deployed for decades, using a liquid electrolyte with low-cost catalysts and cell components.[5] However, the integration of traditional AWE with renewable energy sources has limitations, such as difficulties in load following, low hydrogen discharge pressure, low operating current density, and a highly concentrated alkaline feed.[6–9] A second technology, proton exchange membrane water electrolyzers (PEMWEs), offers higher current density due to the zero-gap approach, pressurized hydrogen discharge, and a similarly long lifetime.[10,11] The perfluorosulfonic acid (PFSA)-based PEM and acidic operating environment, however, requires the use of expensive noble metals, such as platinum and iridium and their oxides,[12] and the large-scale deployment of PEMWEs has been limited by the cost of traditionally overengineered systems and the cost-lifetime tradeoffs associated with platinum group metal thrifting. A third technology, an anion exchange membrane water electrolyzer (AEMWE) is gaining attention due to the possibility of combining the non-acidic pH advantages of an AWE (low-cost components) with those of a PEMWE (high efficiency and pressurized operation).[13–15]

AEMWE technology has noticeably progressed over the past few years, developing AEMs and ionomeric binders, efficient catalyst materials, engineered electrodes and cell designs.[16–21] The MEA consists of a polymer membrane sandwiched between anode and cathode catalyst layers and a porous transport layer (PTL)/gas diffusion layer (GDL) as the outer substrate layers. Catalyst layers may be directly deposited onto the membrane, the configuration called a catalyst-coated-membrane (CCM), or may be coated onto the PTL/GDL, the configuration called a catalyst coated substrate (CCS). With limited data in the literature, CCS-based MEA fabrication with currently available materials has shown slight advantages over a CCM, offering enhanced performance and durability,[22] although there is no firm consensus. Catalyst layer compression, lamination, and formation of ionomeric pathways happen *in situ* during cell operation. Therefore, understanding the cell conditioning process is essential for high performance and durable AEMWE operation. For instance, Lindquist et al.,[23] conditioned the cell in pure water with no soluble supporting electrolyte by applying current from 100 mA/cm^2 to 1.0 A/cm^2 in 100 mA steps, holding for 2 min at

Table 1. Materials used

	Catalyst	Loading (mg/cm^2)	PTL/GDL
Anode	Co_3O_4	3.0 ± 0.1 1.0 ± 0.05	Ni felt (280 μm) SS felt (280 μm)
Cathode	Pt/HSC	0.25 ± 0.05	Toray carbon (290 μm)

each step, and observed a notable difference in the time required for the voltage to reach a steady state. However, less is known about the changes that occur within MEAs during conditioning and the time at which an MEA is fully conditioned. Moreover, water as reactant and produced gases transport depend upon AEM/ionomer properties, PTL/catalyst layer structure, as well as the operating conditions such as feed electrolyte flow rate, mode of operation (dry vs. wet cathode), and so forth. Unlike PEMWE, water is consumed at the cathode and produced at the anode in AEMWE. In PEMWE feed water flow rate has a secondary effect on performance; however, performance is indirectly affected due to temperature changes. Feed water serves as coolant, water for electrolysis, and efficiently removes produced gases. Moreover, dry cathode operation is driven by cost and preferred for pressurized operation at the stack level. In dry cathode AEMWE operation, water diffusion from anode to cathode is critical for performance and durability. Gas saturation and accumulation may block active sites, reduce water and hydroxide ions (OH^-) transport, increase cell resistance, and subsequently decrease cell performance. Pushkareva et al.,[24] studied the effect of flow rate on AEMWE performance, feeding 1 M KOH to both electrodes (cell active area of 7.29 cm^2) and concluded a weak effect of KOH flow rate on performance up to 6 mL/min and observed negative effects at higher flow rates. Azam et al.,[25] compared AEMWE performance feeding KOH in the range of 1, 2, 4, 6, and 9 mL/min (cell active area of 5 cm^2) and concluded an improved performance at a higher flow rate (9 mL/min), attributing enhanced performance to a decrease in cell resistance. The literature survey shows a gap in understanding related to fluid (water and gas) transport effects, performance losses in different modes of operation, and varied electrolyte feed flow rates in each electrode.

In the AEMWE operating environment, the polymer membrane absorbs water and swells, forming an interface with the electrode surface, dictating catalyst utilization and species transport. The transport of OH^- ions in AEM is significantly slower compared to PEM due to the inherent lower mobility of larger ions.[26] Higher AEM conductivity is desirable for the overall efficiency of the AEMWE device. Membrane properties may be manipulated during the film casting process by drying at different temperatures. However, it is critical to understand the drying temperature effects, as it may embrittle and damage the polymer structure. Membrane conductivity is also very sensitive to supporting electrolyte concentration.[17] Jiangjin et al.,[27] modeled the effect of added liquid electrolyte and suggested the formation of an additional electrochemical interface with the electrocatalyst that provides ion-transport pathways and distributes product gas bubbles. The authors suggested that 1.0 M KOH supporting electrolyte feed enhanced a 5-times electrochemical surface area compared to a DI water feed, resulting in significant electrolyzer performance improvement. Therefore, it is essential to monitor the concentration of feed supporting electrolyte during continuous operation to understand the degradation phenomena in MEAs.

In this article, we report, (i) MEA conditioning process linking the cell performance with changes in ohmic and charge transfer resistances, (ii) recoverable voltage loss due to gas bubble accumulation, PTL/bipolar plate surface passivation and changes in oxidation state, (iii) elucidate the effect of feed electrolyte by varying electrolyte flowrate and dry vs. wet cathode feed configurations, (iv) understand AEM films water uptake/swelling properties and their subsequent *in situ* electrochemical performance when dried at different temperatures after casting, and (v) report 700 h cell operation at 1.0 A/cm^2 with insights on performance changes relevant to feed electrolyte concentration changes. As the AEM water electrolysis technology evolves, understanding these phenomena is crucial for the development of efficient and durable systems at a large scale. This study aims to improve our understanding of materials integration and device operation in state-of-the-art MEAs, focusing on the reactants/products' transport.

RESULTS AND DISCUSSION

Membrane-electrode-assemblies conditioning

The materials used in MEA testing are included in Table 1. MEA conditioning is particularly important for catalyst coated substrate (CCS) electrodes, and includes the lamination of the catalyst layer with the AEM, the formation of ionomeric channels in the catalyst layer, and electrocatalyst and membrane activation. The performance of an AEM electrolyzer is generally evaluated by collecting polarization curves,[28,29] which offer a macroscopic view of electrolyzer performance. However, other diagnostics such as EIS, CVs, and so forth, are essential for more detailed information regarding kinetics, transport, and cell components effects in electrolysis.

Conditioning data (presented in Figure 1A) for a CCS-based AEMWE was taken at the beginning of test (BOT) after heating the cell to 80°C and a 100 mA/cm^2 hold for 2 h. The cell current density was then increased to 500 mA/cm^2 and ramped up to 3 A/cm^2, holding 5 h at each current density (Figure 1A). Polarization and EIS data were collected before and after each current density hold, and the cell voltage appears to decrease during the 500 mA/cm^2 hold and then stabilize with very little change at higher current densities (see Figure 1B). The performance noticeably improves after the 500 mA/cm^2 hold (current density increases from 2.8 A/cm^2 to 3.6 A/cm^2 at 2 V as can be seen in polarization curves), with no further improvement after the 2.0 or 3.0 A/cm^2 holds, suggesting the completion of the conditioning process. EIS plots (see Figure 1C), illustrate the corresponding decrease in the HFR and charge transfer resistances after the 500 mA/cm^2 hold, which stabilize after subsequent holds. At 1.80 V, impedance measurements show a decrease in HFR from 0.015 Ω (75 mΩ cm^2) to 0.013 Ω (65 mΩ cm^2), and the charge transfer resistance reduces from 0.0098 Ω (49 mΩ cm^2) to 0.0072 Ω (36 mΩ cm^2) after the first hold. The decrease in HFR suggests AEM activation, likely due to complete ion exchange (replacing bicarbonate with hydroxide) and the formation of ionic transport channels. Post test membrane thickness

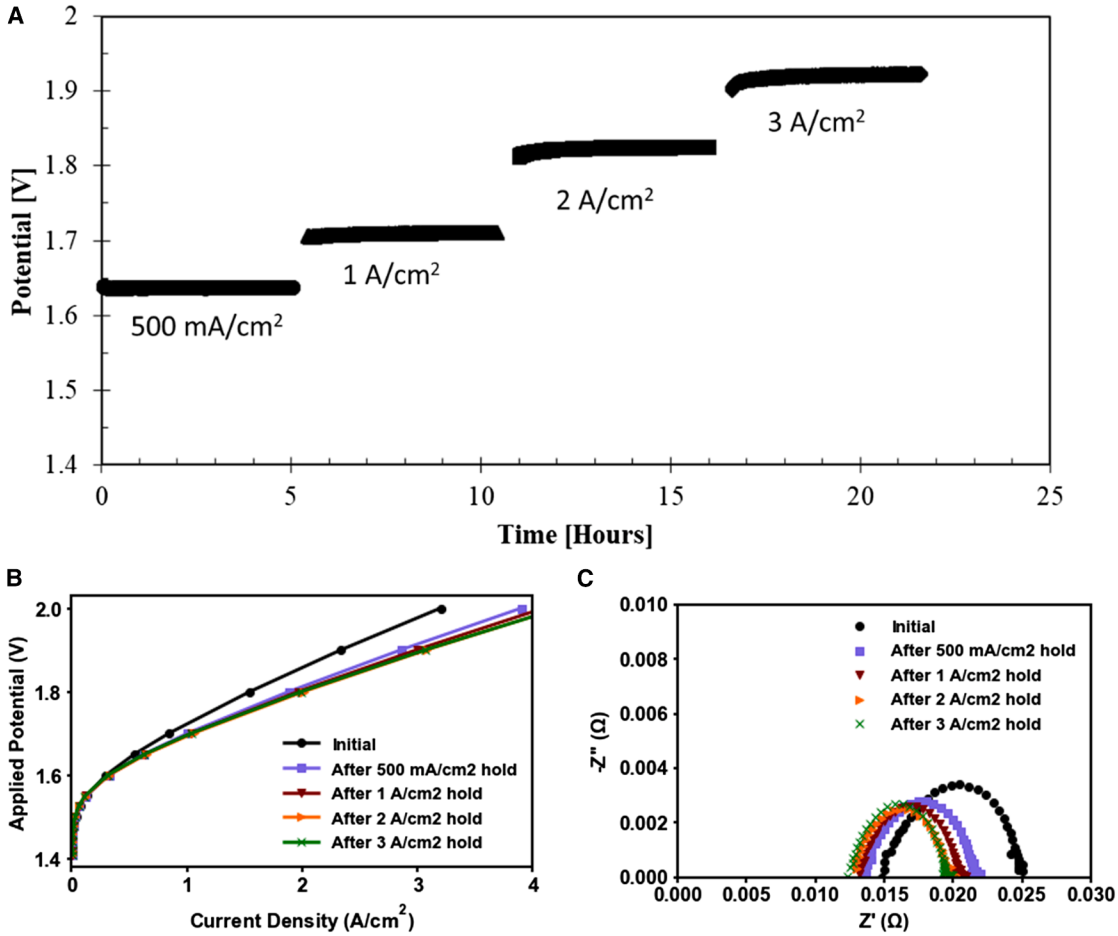

Figure 1. MEA conditioning, test results, and impedance spectra with a symmetrical, fixed flow rate

(A–C) MEA activation process shows (A). Different current density holds 5 h each, (B). Polarization plots comparing BOT and the end of each current density hold, (C). EIS plots at 1.80 V comparing BOT and the end of each current density hold. [AEM: Piperlon 80 μm, Ionomer: Piperlon dispersion, anode: Co_3O_4 deposited on Ni PTL, cathode: Pt/HSC deposited on carbon paper, 1 M KOH fed to both electrodes with flow rate of 50 mL/min at 80°C and ambient pressure].

measurements show no membrane thickness changes during this short-term conditioning operation, suggesting that there is no noticeable membrane thinning. The decrease in charge transfer resistance suggests improved site access, interfacial contact with the catalyst layer, catalyst layer lamination with the AEM, and the formation of ionomeric channels within the catalyst layer for improved H_2O/OH^- ions transport. The voltage breakdown analysis, including ohmic, kinetic, and catalyst layer overpotential contributions, is illustrated in Figure S1. The main contribution to the improved performance during conditioning is a reduction in the catalyst layer resistance, while the kinetic and ohmic overpotentials remained unchanged. Figure S1D compares the CVs collected following BOT and the 3.0 A/cm^2 hold; minimal changes to the CVs suggest no major changes in site-access (electrochemical surface area).

The voltage increased at the start of the 2.0 and 3.0 A/cm^2 current density holds and then stabilized, which was not observed at 500 mA/cm^2 (see Figure 2). This initial increase in voltage at high current density is likely in part due to gas bubble accumulation, which covers active sites through a local transport issue at high current density. This voltage loss, however, was recoverable after a short respite or cycling the cell and is not captured in polarization curves (Figure 1B). This loss could be linked to PTL structural properties and catalyst layer porosity, dictating gas/water transport.

Additionally, the reversible voltage loss could also be partially due to a change in the catalyst (cobalt) oxidation state or PTL/bipolar plate surface passivation. While cycling the cell between 0 and 1.4 V is beneficial to voltage recovery, it abruptly increases when resuming high current density operation. This finding is further demonstrated in Figure S2, which compares the voltage response under a 1 A/cm^2 hold, when CVs are or are not taken. In the case of CV collection, the voltage initially recovers but abruptly degrades.

Effect of electrolyte flow rate

To understand the importance of gas removal and water transport, the AEMWE was operated by varying the cathode flow rate while keeping the anode flow rate constant at 50 mL/min (see Figure 3) and then decreasing the cathode flow rate from

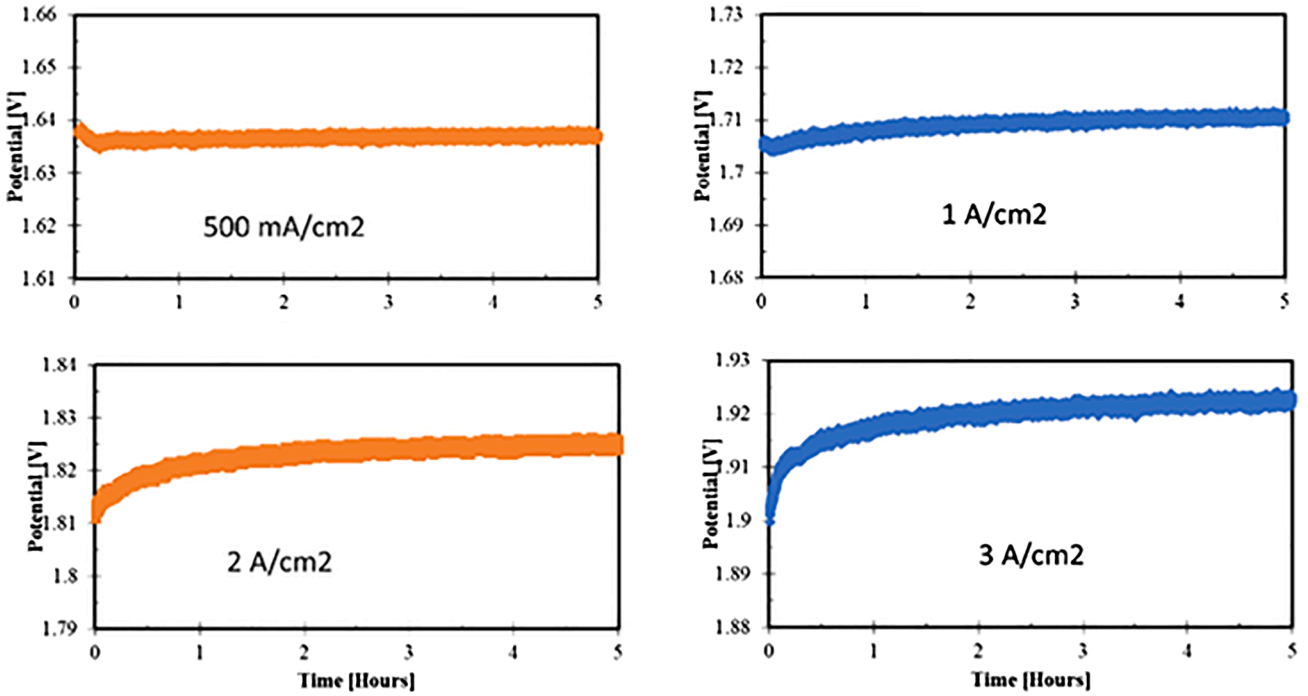

Figure 2. Voltage response at various current densities show an increase in initial voltage loss with increasing current density

50 mL/min to 10 mL/min with a step of 10 mL/min. EIS plots in Figure 3B further illustrate an increase in charge transfer resistance with a decrease in the cathode flow rate. In wet cathode operation, the continued electrolyte flow likely helps remove the produced hydrogen from the cathode. At the lower flow rate, the residence time of produced hydrogen increases, blocking the catalyst active sites and potentially increasing the local gas partial pressure, hindering water and OH^- transport to/from active sites. In contrast to a dry cathode, feeding liquid electrolyte to the cathode side causes more H_2 bubbles to be trapped in the electrode. Due to plenty of liquid water in the cathode, enhanced bubble generation can decrease accessibility to more catalyst sites and distort the conductive ionic path toward the AEM.

Next, changing the anode flow rate while keeping the cathode flow rate constant did not show a significant impact on cell performance (see Figure 4). HFR, as well as charge transfer resistances, also did not noticeably change in this case. Compared to changes at the cathode, differences in the anode flow rate result in smaller performance changes and may have been impacted by the high porosity and fiber to fiber distance of the anode PTL.

In the third case, decreasing the anode flow rate with a dry cathode also had a negative impact on cell performance, and

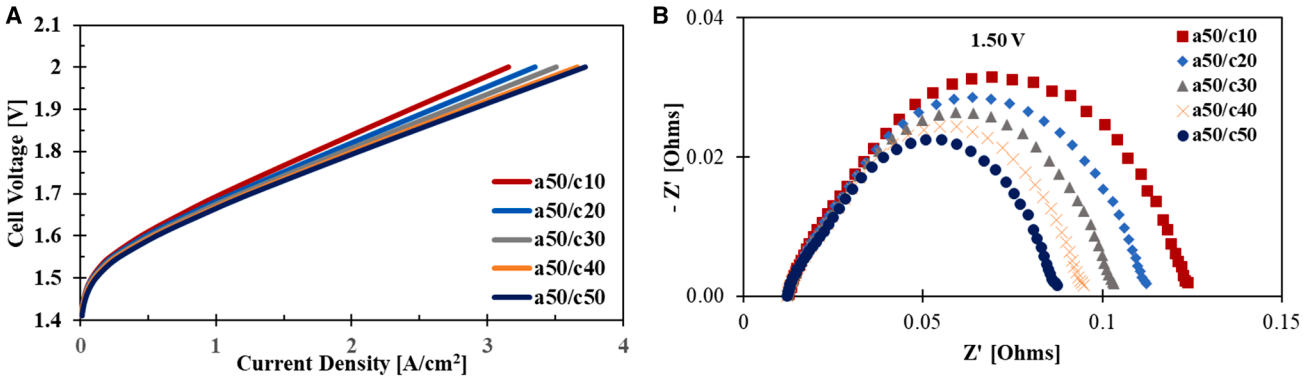

Figure 3. MEA test results and impedance spectra while varying the cathode flow rate

(A and B). Polarization plots varying cathode feed flow rate (1M KOH) while keeping the anode flow rate constant, (B). corresponding EIS plots at 1.50 V, varying cathode flow rate, keeping anode flow rate constant. [AEM: Piperlon 80 μm, Ionomer: Piperlon dispersion, anode: Co_3O_4 deposited on Ni PTL, cathode: Pt/HSC deposited on carbon paper, 1 M KOH variable feed at 80°C and ambient pressure].

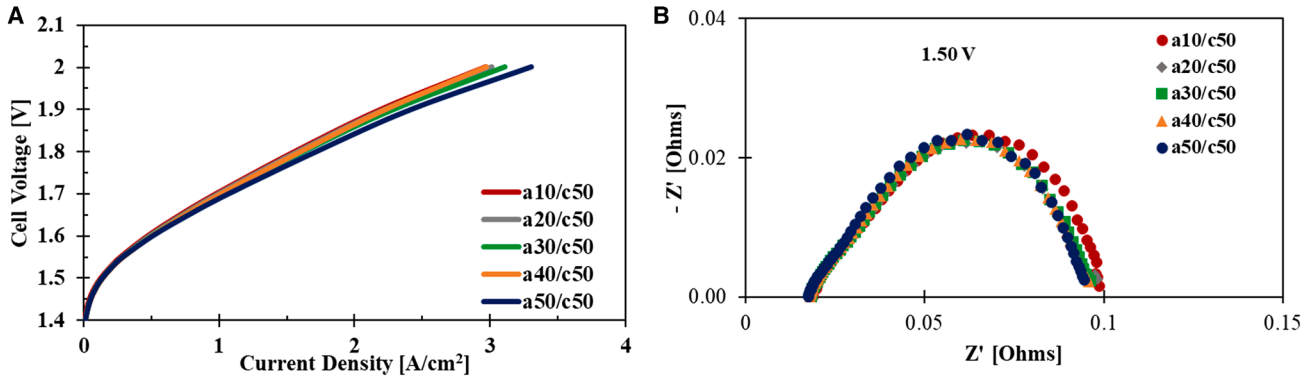

Figure 4. MEA test results and impedance spectra while varying the anode flow rate

(A and B) Cell performance shows (A). polarization plots varying anode feed flow rate (1M KOH) while keeping the cathode flow rate constant and (B). corresponding EIS plots at 1.50 V, varying anode flow rate, keeping cathode flow rate constant. [AEM: Piperlon 80 μm, Ionomer: Piperlon dispersion, anode: Co_3O_4 deposited on Ni PTL, cathode: Pt/HSC deposited on carbon paper, 1 M KOH variable feed at 80°C and ambient pressure].

further resulted in an increase in the charge transfer resistance (see Figure 5). Feeding electrolyte to only the anode side is beneficial due to easy gas removal, and secondly, the concentration gradient between anode and cathode could likely be higher for an anode feed only case, which means better mass transport. The voltage breakdown of anode feed only shows lower kinetic as well as residual losses compared to the wet cathode configuration, suggesting increased catalyst utilization and enhanced transport as observed by Tricker et al.[30] The catalyst layer resistance remained unchanged in both configurations. With a decrease in anode flow rate, the concentration gradient also decreased, hindering the water transport to the cathode as well as slowing the removal of O_2 bubbles.

Effect of membrane thickness

In AEMWE, the membrane thickness directly affects OH^- ions and water transport. Particularly in water-only feeds, a thinner membrane may help transport water to the cathode during dry operation. However, in supporting electrolytes, the membrane thickness can be less critical to cell performance, outside of ohmic/HFR differences. Figure 6 compares the performances of a 40 and 80 μm Piperlon AEM, which are consistent with expectations.

Effect of the membrane drying process

Membrane water uptake and swelling play important roles in cell performance, and one way to control water uptake is by drying (curing) the films after casting. Here, we discuss the results of three cast membrane films by varying the drying temperature and evaluating their *ex situ* as well as *in situ* electrochemical performance (see Figure S3 for casting and drying process). To understand the effects of polymer processing on AEM characteristics, the film samples were tested for IEC, water uptake, and conductivity with the procedure outlined in the experimental section. Higher *ex situ* properties of undried AEM may lead to a higher degree of dimensional swelling, which increases the diffusion path for water and ionic transport, leading to lower site access and higher charge transfer resistances. Higher degrees of membrane swelling and the resulting higher charge transfer resistance may thereby dominate the slight benefits of lower

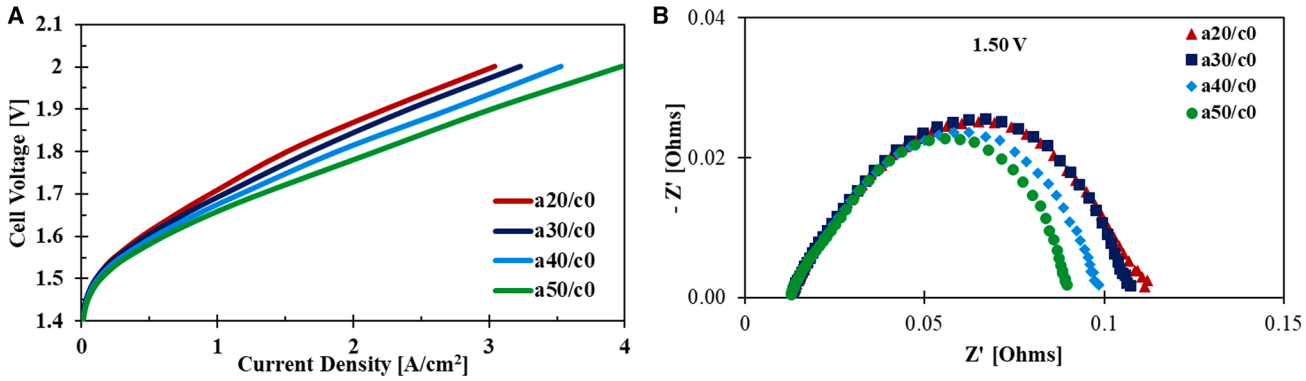

Figure 5. MEA test results and impedance spectra while varying the anode flow rate under a dry cathode condition

(A and B). Polarization plots varying anode feed flow rate (1M KOH) with dry cathode (B). Corresponding EIS plots at 1.50 V, varying the anode flow rate with a dry cathode. [AEM: Piperlon 80 μm, Ionomer: Piperlon dispersion, anode: Co_3O_4 deposited on Ni PTL, cathode: Pt/HSC deposited on carbon paper, 1 M KOH variable feed at 80°C and ambient pressure].

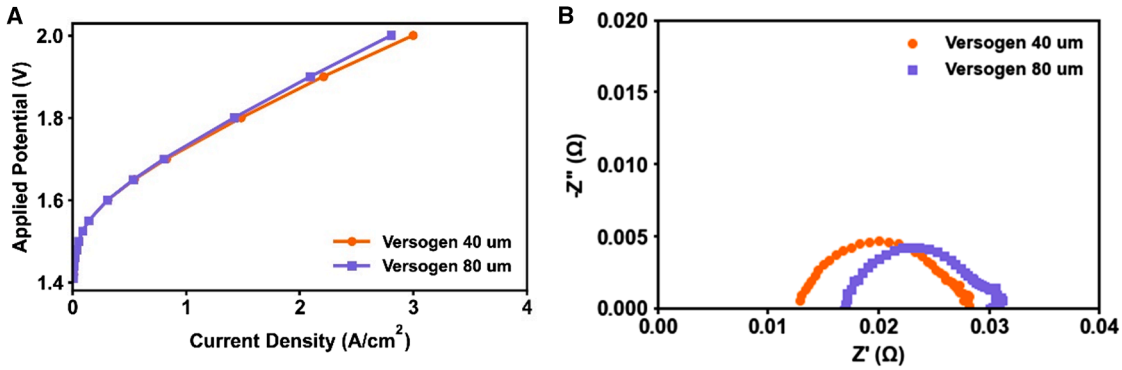

Figure 6. MEA test results and impedance spectra while varying the membrane thickness

(A and B). Polarization plots compare Piperlon 40 μm thick membrane with 80 μm, (B). Corresponding EIS plots at 1.80 V with varying thickness. [AEM: Piperlon 40 μm and 80 μm, Ionomer: Piperlon dispersion, anode: Co_3O_4 deposited on Ni PTL, cathode: Pt/HSC deposited on carbon paper, 1 M KOH fed to both electrodes at 80°C and ambient pressure].

HFR, higher IEC, and conductivity, and negatively impact cell efficiency.

The *ex situ* characterization data, including IEC, water uptake, and ionic conductivity, is presented in Figure 7. The undried AEM had an IEC value of 1.58 meq/g, which was reduced to 1.37 meq/g when dried at 60°C and further reduced to 1.17 meq/g when dried at 80°C. Similar patterns were observed for liquid water uptake, where the value decreased when dried at both drying temperatures. While the undried AEM also appeared to yield the best conductivity, the dried AEM samples both yield relatively similar results. The dimensional swelling measurements were taken at 80°C for the three AEM samples in 1 M KOH (see Figure 7D). The undried AEM significantly showed higher swelling (in thickness mode).

In the electrochemical performance evaluation (see Figure 8A), the AEM sample dried at 60°C had the highest performance, yielding a current density of 3.6 A cm^{-2} at 2.0 V, compared to the undried AEM (3.1 A cm^{-2}) and dried at 80°C (2.7 A cm^{-2}). Voltage breakdown analysis is typically performed to evaluate the individual overpotential contribution toward ohmic and kinetic losses.[31,32] All three samples contributed fairly similarly to the ohmic losses, which were in line with the corresponding HFR results (see Figure S4). The undried AEM showed relatively higher kinetic overpotential, coupled with a higher charge transfer resistance. Due to the lower swelling of the dried AEMs, the membrane-electrode interface likely contributed to a reduced charge transfer resistance (lower residual loss). The catalyst layer resistance contribution of undried MEA was slightly lower compared to dried samples.

The Nyquist plots from EIS measurements collected at 1.50 V are overlaid for comparison (see Figure 8B). The undried sample yielded a slightly lower HFR of 0.0125 Ω (62.5 mΩ cm^2) compared to 0.0146 Ω (73.0 mΩ cm^2) and 0.0142 Ω (73.1 mΩ cm^2) for dried at 60°C and 80°C, respectively. The charge transfer resistance (R_{CT}), on the other hand, was higher for undried samples (0.1275 Ω or 637.5 mΩ cm^2) compared to (0.0754 Ω or 377.1 mΩ cm^2) and (0.0855 Ω or 427.3 mΩ cm^2) for dried AEMs at 60°C and 80°C, respectively. Higher R_{CT} may have a significant effect on cell performance as the charge transfer is overwhelmed by the reaction kinetics.[33] The undried sample had a higher water uptake, which resulted in higher dimensional swelling. It was likely that the swollen membrane polymer covered active sites at the membrane-electrode interface, resulting in the reduced activity and mobility of charges as depicted by higher charge transfer resistance. Moreover, lower electrochemical surface area (ECSA) results from CVs also support the slower activity due to swelled polymer covering the catalyst sites at the interface (see Figure S4D). The slightly lower catalyst layer resistance of the undried AEM, on the other hand, could be explained by enhanced contact between ionomer paths with the membrane at the interface. The lower ECSA of undried AEM compared to dried AEMs was in line with the higher charge transfer resistance and higher kinetic overpotential contribution.

Anion exchange membrane electrolyzer single cell durability

The voltage response of the cell over 700 + h hold at 1.0 A/cm^2 is presented in Figure 9A. For this durability experiment, a SS PTL purchased from Bekaert (15FP3 - 310 μm thick and 75% porosity) was employed to enhance water and gas transport through the PTL inspired by the high performance reported by Tricker et al.,[34] At 1.0 A/cm^2, the cell voltage was 1.66 V at BOT; however, it increased to around 1.82 V within a few hours of operation. This initial increase in cell voltage (160 mV) was higher than for a Ni PTL, when tested with the same MEA (an increase of over 100 mV) in steady-state operation. Following this initial increase, the voltage gradually decreased over time. After 160 h, the cell stopped due to a power failure; following a restart, a polarization curve overlapped with the BOT, suggesting that there was no irreversible degradation in performance. When resuming operation at 1.0 A/cm^2, the voltage continued to gradually decrease. Polarization (see Figure 9B) and EIS measurements (see Figure 9C) were taken after 400 and 650 h and compared with the BOT measurements, where improvement in performance, decrease in HFR, and an increase in R_{CT} are observed. Voltage breakdown analysis was done to

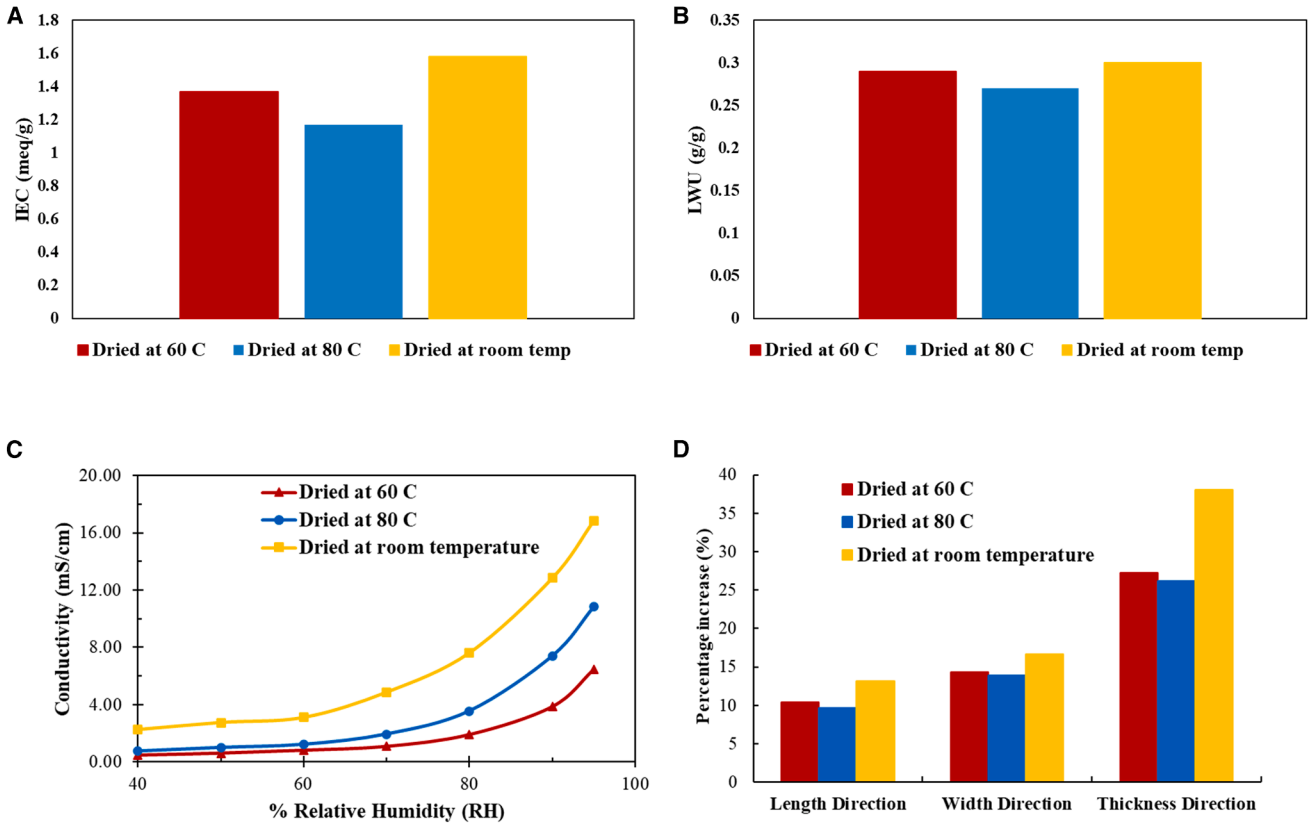

Figure 7. *Ex situ* characterization of custom polymer films

(A–D). Ion exchange capacity (IEC) comparison of undried vs. dried samples, (B). liquid water uptake (LWU) of dried vs. undried samples, (C). conductivity comparing undried vs. dried samples, and (D). dimensional swelling of dried vs. undried samples soaked in 1.0 M KOH for 1 h at 80°C.

evaluate the overpotential contribution coming from each MEA component (see Figure S5). The catalyst layer resistance decreased over time, which was potentially due to catalyst layer compression and changes in catalyst layer structure, the formation of ionomeric pathways, or ionomer oxidation, freeing up catalyst particles for enhanced activity and improving performance. The ohmic contribution to overpotential decreases over time and is consistent with the decrease in HFR. Moreover, residual loss increases over time, likely due to changes in the catalyst layer structure affecting transport.

The HFR-free potential comparison suggests that no significant contribution came from the electrodes and points to the improved membrane conductivity as the reason for the decreased HFR. Enhanced conductivity could be due to membrane thinning or

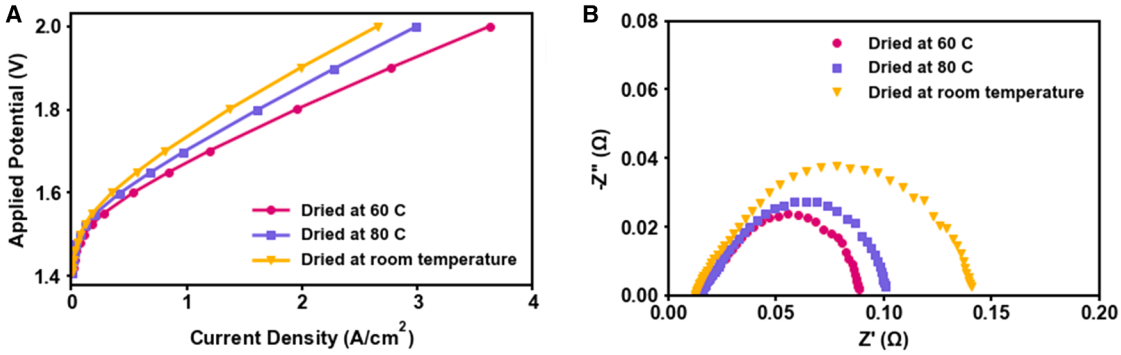

Figure 8. MEA test results and impedance spectra while varying the polymer drying temperature

(A and B) Polarization plots compare the I-V response of undried vs. dried AEM samples, (B) EIS spectra collected at 1.50 V overlayed for three AEM samples. [AEM: custom polymer, Ionomer: custom polymer dispersion, anode: Co_3O_4 deposited on Ni PTL, cathode: Pt/HSC deposited on carbon paper, 1 M KOH fed to both electrodes at 80°C and ambient pressure].

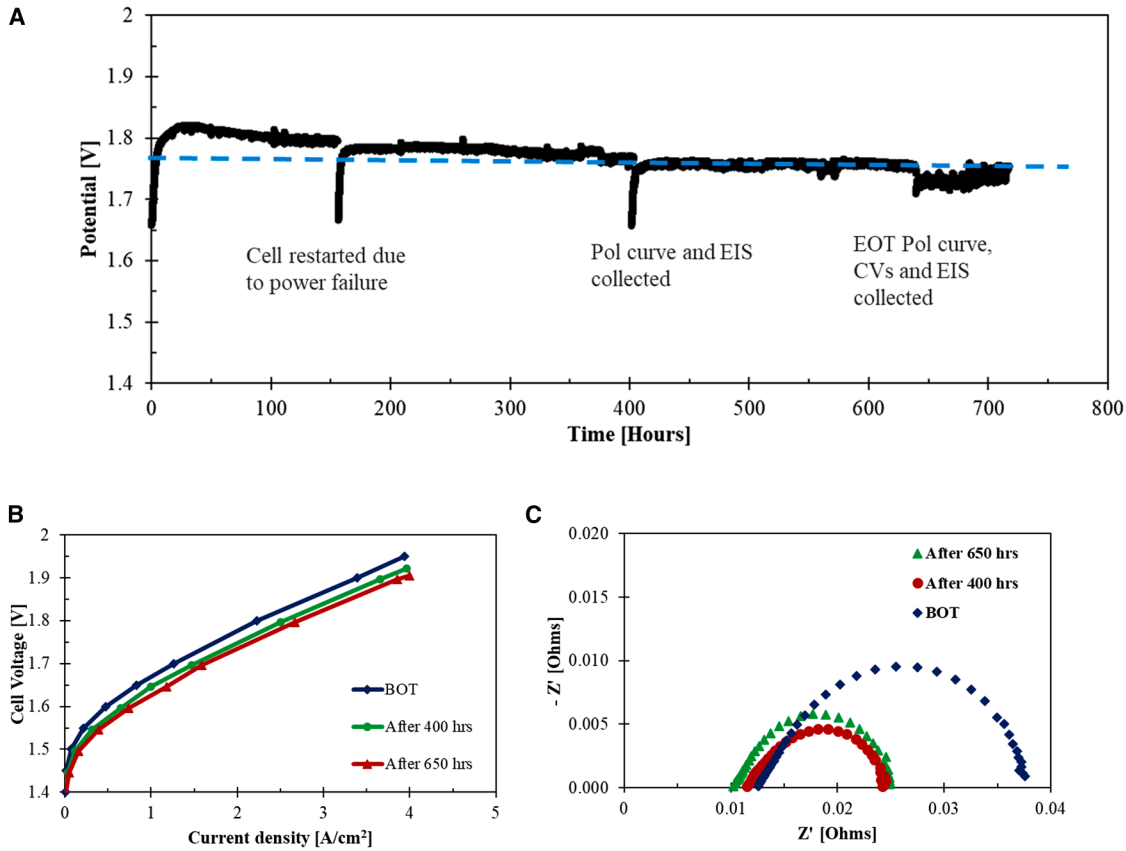

Figure 9. MEA test results and impedance spectra during a 1.0 A/cm^2 durability test

(A and B). Durability at 1.0 A/cm^2 holds for dried AEM at 60°C for 72 h using Co_3O_4 deposited on stainless steel PTL as anode and PtC deposited on Toray carbon paper as cathode, (B). BOT and EOT polarization scans comparison, (C). corresponding EIS collected at 1.80 V [AEM: custom polymer dried at 60°C, 50 μm thick, ionomer: custom polymer dispersion, anode: Co_3O_4 deposited on SS PTL, cathode: Pt/HSC deposited on carbon paper, 1.0 M KOH fed to both electrodes at 80°C and ambient pressure].

an increase in the KOH concentration over time as we replenished the electrolyte every few days. For membrane thinning, the thickness of the tested membrane was measured using a micrometer and showed no noticeable change compared with the untested membrane. pH measurements of circulated 1.0 M KOH solutions taken at BOT (13.92), after 400 h(14.14), and after 650 h (14.39), however, suggest that the pH of 14.39 corresponds to approx. 2.0 M (doubled compared to BOT). These measurements clearly show an increase in KOH concentration over time, responsible for enhanced membrane conductivity.

Effect of supporting electrolyte on cell performance

Based on pH measurements discussed for durability data, it is relevant to state the importance of supporting electrolytes in AEMWE performance as reported in the literature.[17] Figure 10A compares polarization responses of AEMWE cells operated with 1.0 M KOH, 0.1 M KOH, and DI water feeds. Cell performance drastically improves when operated with 0.1 M KOH supporting electrolyte compared to DI water feed, and significantly lowered HFR as well as R_{CT} (see Figure 10B). At 2.0 V, the current density was 0.18 A/cm^2 with DI water feed, which was 2.51 A/cm^2 with 0.1 M KOH, and even higher 4.19 A/cm^2 with 1.0 M KOH feed. The HFR decreased from ~0.1 Ω (500 mΩ cm^2) to 0.0229 Ω (114.5 mΩ cm^2) when switched from DI water to 0.1 M KOH and further decreased to 0.0158 Ω (79 mΩ cm^2) with 1.0 M KOH feed. The corresponding charge transfer resistances were 0.435 Ω (2175 mΩ cm^2), 0.013 Ω (65 mΩ cm^2), and 0.0057 Ω (28.5 mΩ cm^2) with DI water, 0.1 M KOH, and 1.0 M KOH feeds, respectively. Therefore, it is essential to control the pH (concentration) of supporting electrolyte feeds while comparing the performance/durability of different polymers employed in AEMWE.

Constant current operation at various current densities was employed for conditioning the MEAs. The cell performance was noticeably improved after the first hold, and the cell voltage stabilized in subsequent current holds. Corresponding impedance measurements showed a decrease in HFR as well as a decrease in the charge transfer resistance after the first hold. This performance improvement is attributed to a decrease in catalyst layer resistance due to compression in the cell and enhanced membrane conductivity during continuous operation. The initial voltage loss observed at higher current density hold could be associated with bubble accumulation blocking active sites (kinetics) and affecting transport (water and ionic). For 1.0 M KOH

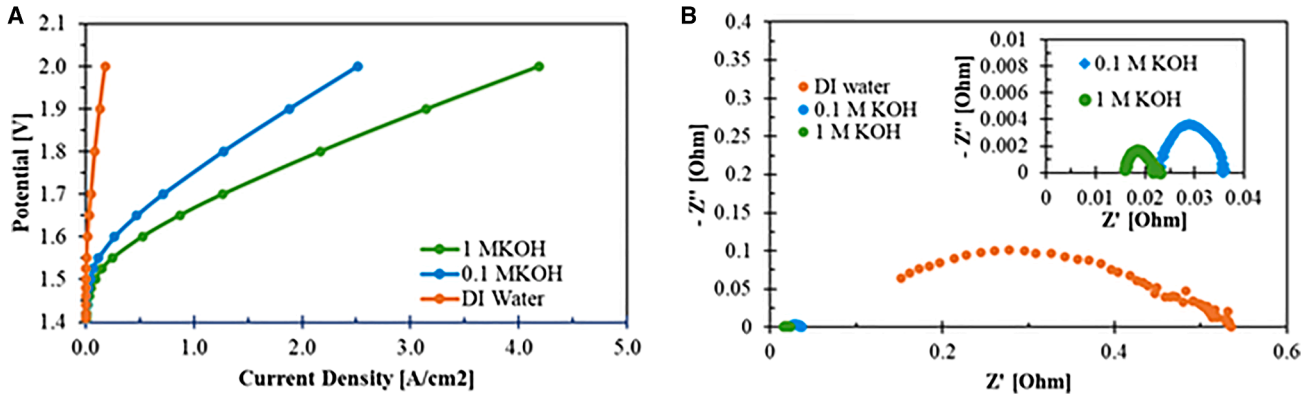

Figure 10. MEA test results and impedance spectra in water and different concentrations of supporting electrolyte

(A and B). Polarization plots compare DI water operation vs. 0.1 and 1 M KOH supporting electrolyte feed, (B). corresponding EIS Nyquist plots at 1.50 V comparing impedance with DI water, 0.1 M, and 1 M KOH feed (inset zoomed in Nyquist plot). [AEM: PiperIon 80 μm, Ionomer: PiperIon dispersion, anode: Co_3O_4 deposited on SS PTL, cathode: Pt/HSC deposited on carbon paper, 1.0 M KOH fed to both electrodes at 80°C and ambient pressure].

electrolyte feeds, the cell performance was negatively affected by lowering the cathode flow rate while keeping the anode flow rate constant. Dry cathode operation was further beneficial, potentially due to the enhanced transport of gas, water, and OH^- ions. Only a reduction in the anode flow rate did not have a noticeable effect on cell performance. In a 1.0 M KOH system, commercial Verosgen 40 μm AEM performed slightly better than 80 μm thick AEM with noticeably lower HFR. The homemade AEM dried at 60°C after casting showed reduced water uptake and swelling, enhancing the cell performance. The major contribution in performance enhancement was due to reduced charge transfer resistance in the drying process. However, drying the membrane at a higher temperature (80°C) was not effective, likely due to changes in the mechanical properties of the polymer film. Finally, a 700-h durability test with all commercial materials shows improved performance over time. HFR was reduced over time, suggesting enhanced ionic conductivity, whereas the electrolyte pH was increased responsible for this performance gain. Finally, the DI water feed operation was compared with 0.1 M KOH and 1.0 M KOH feeds, emphasizing the sensitivity of ionic conductivity in different electrolyte feeds. Therefore, pH of electrolyte or conductivity control is needed for durability experiments to eliminate the effects of KOH concentration changes. With the evolution of AEM water electrolysis technology, understanding the device operation is crucial for the development of efficient and durable systems. This study aims to improve our understanding of materials integration and device operation in state-of-the-art MEAs, focusing on the reactants/products transport.

Limitations of the study

This study is limited to electrochemical characterization (performance/short-term durability) of AEM single cells with varying operating conditions only. Catalyst inks, rheology, electrode structures, and postmortem analysis using SEM/STEM are not covered. The authors aim to investigate AEMWE durability with steady-state or voltage/current cycling and support with postmortem analysis in the near future.

RESOURCE AVAILABILITY

Lead contact

Further information and requests for resources and reagents should be directed to and will be fulfilled by the lead contact, Shaun Alia (shaun.alia@nrel.gov).

Materials availability

This study did not generate new unique reagents.

Data and code availability

- This study generated data through single-cell tests and diagnostics. Data are available upon request.
- This study did not generate code.
- Any additional information required to reanalyze the data reported in this article is available from the lead contact upon request.

ACKNOWLEDGMENTS

We acknowledge financial support from the U.S. Department of Energy, Small Business Innovation Research program. The polymers leveraged in this work were developed with support by the U.S. Department of Energy, Office of Science, Basic Energy Sciences. This work was authored by the National Renewable Energy Laboratory, operated by Alliance for the Sustainable Energy, LLC, for the U.S. Department of Energy (DOE) under Contract No. DE-AC36-08GO28308. The views expressed in the article do not necessarily represent the views of the DOE or the U.S. Government. The U.S. Government retains, and the publisher, by accepting the article for publication, acknowledges that the U.S. Government retains a nonexclusive, paid-up, irrevocable, worldwide license to publish or reproduce the published form of this work, or allow others to do so, for U.S. Government purposes.

AUTHOR CONTRIBUTIONS

N.U. Hassan performed electrochemical performance, durability measurements, analysis, and prepared the article. R. Iyer prepared polymer dispersions, cast films, and dried. A. Boudreau and A. Palau performed *ex situ* characterization of polymer films. C. Parrish planned the polymer film compositions and guided film fabrication processes. S. Mauger and B. S. Pivovar advised overall objectives of the study. S. M. Alia edited and supervised the overall article.

DECLARATION OF INTERESTS

The authors declare no competing interests.

STAR★METHODS

Detailed methods are provided in the online version of this paper and include the following:

- KEY RESOURCES TABLE
- METHOD DETAILS
  - Polymer membranes and ionomer
  - Ex-situ characterization of polymer films
  - Electrode fabrication
  - Membrane electrode assembly and testing
- QUANTIFICATION AND STATISTICAL ANALYSIS

SUPPLEMENTAL INFORMATION

Supplemental information can be found online at https://doi.org/10.1016/j.isci.2025.114037.

Received: December 5, 2024
Revised: July 3, 2025
Accepted: November 10, 2025
Published: November 17, 2025

REFERENCES

1. Blakers, A., Stocks, M., Lu, B., and Cheng, C. (2021). The observed cost of high penetration solar and wind electricity. Energy *223*, 121150.
2. Khare, V., Nema, S., and Baredar, P. (2016). Solar–wind hybrid renewable energy system: A review. Renew. Sustain. Energy Rev. *58*, 23–33.
3. Li, K., Bian, H., Liu, C., Zhang, D., and Yang, Y. (2015). Comparison of geothermal with solar and wind power generation systems. Renew. Sustain. Energy Rev. *42*, 1464–1474.
4. Decourt, B., Lajoie, B., Debarre, R., and Soupa, O. (2014). Hydrogen Based Energy Conversion (Houston, TX, USA: The SBC Energy Institute).
5. Medina, E., and Pinter, B. (2020). Electron Density Difference Analysis on the Oxidative and Reductive Quenching Cycles of Classical Iridium and Ruthenium Photoredox Catalysts. J. Phys. Chem. A *124*, 4223–4234.
6. Li, D., Motz, A.R., Bae, C., Fujimoto, C., Yang, G., Zhang, F.Y., Ayers, K.E., and Kim, Y.S. (2021). Energy Environ. Sci. *21*, 3393.
7. Ayers, K.E., Anderson, E.B., Capuano, C.B., Niedzwiecki, M., Hickner, M.A., Wang, C.Y., Leng, Y., and Zhao, W. (2013). Characterization of Anion Exchange Membrane Technology for Low Cost Electrolysis. ECS Trans. *45*, 121–130.
8. Abbasi, R., Setzler, B.P., Lin, S., Wang, J., Zhao, Y., Xu, H., Pivovar, B., Tian, B., Chen, X., Wu, G., and Yan, Y. (2019). A Roadmap to Low-Cost Hydrogen with Hydroxide Exchange Membrane Electrolyzers. Adv. Mater. *31*, 1805876.
9. Godula-Jopek, A. (2015). Hydrogen Production: By Electrolysis (John Wiley & Sons).
10. Ayers, K.E., Anderson, E.B., Capuano, C., Carter, B., Dalton, L., Hanlon, G., Manco, J., and Niedzwiecki, M. (2010). ECS Trans. *3*, 33.
11. Rashid, M.M., Mesfer, M.K.A., Naseem, H., and Danish, M. (2015). Int. J. Eng. Adv. Technol. *4*, 2249–8958.
12. Carmo, M.F., Fritz, D.L., Mergel, J., and Stolten, D. (2013). Int. J. Hydrogen Energy *38*, 901–4934.
13. Götz, M., Lefebvre, J., Mörs, F., Koch, A.M., Graf, F., Bajohr, S., Reimert, R., and Kolb, T. (2016). Renew. Energy *85*, 1371.
14. Lim, A., Cho, M.K., Lee, S.Y., Kim, H.J., Yoo, S.J., Sung, Y.E., Jang, J.H., Park, H.S., and Electrochem, J. (2017). A Review of Industrially Developed Components and Operation Conditions for Anion Exchange Membrane Water Electrolysis. Sci. Technol. *8*, 265–273.
15. Schmidt, O., Gambhir, A., Staffell, I., Hawkes, A., Nelson, J., and Few, S. (2017). Future cost and performance of water electrolysis: An expert elicitation study. Int. J. Hydrogen Energy *42*, 30470–30492.
16. Hassan, N.U., Mandal, M., Zulevi, B., Kohl, P.A., and Mustain, W.E. (2022). Understanding and improving anode performance in an alkaline membrane electrolyzer using statistical design of experiments. Electrochim. Acta *409*, 140001.
17. Hassan, N.U., Zheng, Y., Kohl, P.A., and Mustain, W.E. (2022). KOH vs Deionized Water Operation in Anion Exchange Membrane Electrolyzers. J. Electrochem. Soc. *169*, 044526.
18. Hassan, N.U., Motyka, E., Kweder, J., Ganesan, P., Brechin, B., Zulevi, B., Colón-Mercado, H.R., Kohl, P.A., and Mustain, W.E. (2023). Effect of porous transport layer properties on the anode electrode in anion exchange membrane electrolyzers. J. Power Sources *555*, 232371.
19. Huang, G., Mandal, M., Hassan, N.U., Groenhout, K., Dobbs, A., Mustain, W.E., and Kohl, P.A. (2021). J. Electrochem. Soc. *168*, 24503.
20. Huang, G., Mandal, M., Hassan, N.U., Groenhout, K., Dobbs, A., Mustain, W.E., and Kohl, P.A. (2020). Ionomer Optimization for Water Uptake and Swelling in Anion Exchange Membrane Electrolyzer: Oxygen Evolution Electrode. J. Electrochem. Soc. *167*, 164514.
21. Hua, D., Huang, J., Fabbri, E., Rafique, M., and Song, B. (2023). Development of Anion Exchange Membrane Water Electrolysis and the Associated Challenges: A Review. Chemelectrochem *10*, 202200999.
22. Koch, S., Metzler, L., Kilian, S.K., Heizmann, P.A., Lombeck, F., Breitwieser, M., and Vierrath, S. (2023). Toward Scalable Production: Catalyst-Coated Membranes (CCMs) for Anion-Exchange Membrane Water Electrolysis via Direct Bar Coating. Adv. Sustain. Syst. *7*, 2200332.
23. Lindquist, G.A., Oener, S.Z., Krivina, R., Motz, A.R., Keane, A., Capuano, C., Ayers, K.E., and Boettcher, S.W. (2021). Performance and Durability of Pure-Water-Fed Anion Exchange Membrane Electrolyzers Using Baseline Materials and Operation. ACS Appl. Mater. Interfaces *13*, 51917–51924.
24. Pushkareva, I.V., Solovyev, M.A., Butrim, S.I., Kozlova, M.V., Simkin, D.A., and Pushkarev, A.S. (2023). Membranes *13*, 192.
25. Azam, A.M.I.N., Ragunathan, T., Zulkefli, N.N., Masdar, M.S., Majlan, E.H., Yunus, R.M., Shamsul, N.S., Husaini, T., and Shaffee, S.N.A. (2023). Polymers *15*, 1301.
26. Hibbs, M.R., Hickner, M.A., Alam, T.M., McIntyre, S.K., Fujimoto, C.H., and Cornelius, C.J. (2008). Transport Properties of Hydroxide and Proton Conducting Membranes. Chem. Mater. *20*, 2566–2573.
27. Liu, J., Kang, Z., Li, D., Pak, M., Alia, S.M., Fujimoto, C., Bender, G., Kim, Y.S., and Weber, A.Z. (2021). Elucidating the Role of Hydroxide Electrolyte on Anion-Exchange-Membrane Water Electrolyzer Performance. J. Electrochem. Soc. *168*, 054522.
28. Wu, X., and Scott, K. (2014). J. Power Sources *214*, 124–129.
29. Miller, A., Singh, L., Wang, L., and Liu, H. (2019). Linking internal resistance with design and operation decisions in microbial electrolysis cells. Environ. Int. *126*, 611–618.
30. Tricker, A.W., Lee, J.K., Shin, J.R., Danilovic, N., Weber, A.Z., and Peng, X. (2023). Design and operating principles for high-performing anion exchange membrane water electrolyzers. J. Power Sources *567*, 232967.
31. Volk, E.K., Kwon, S., and Alia, S.M. (2023). Catalytic Activity and Stability of Non-Platinum Group Metal Oxides for the Oxygen Evolution Reaction in Anion Exchange Membrane Electrolyzers. J. Electrochem. Soc. *170*, 064506.
32. Padgett, E., Bender, G., Haug, A., Lewinski, K., Sun, F., Yu, H., Cullen, D.A., Steinbach, A.J., and Alia, S.M. (2023). Catalyst Layer Resistance and Utilization in PEM Electrolysis. J. Electrochem. Soc. *170*, 084512.
33. Najafi, B., Bonomi, P., Casalegno, A., Rinaldi, F., and Baricci, A. (2020). Rapid Fault Diagnosis of PEM Fuel Cells through Optimal Electrochemical Impedance Spectroscopy Tests. Energies *13*, 3643.
34. Tricker, A.W., Ertugrul, T.Y., Lee, J.K., Shin, J.R., Choi, W., Kushner, D.I., Wang, G., Lang, J., Zenyuk, I.V., Weber, A.Z., and Peng, X. (2023). Pathways Toward Efficient and Durable Anion Exchange Membrane Water Electrolyzers Enabled By Electro-Active Porous Transport Layers. Adv. Energy Mater. *14*, 2303629.

STAR★METHODS

KEY RESOURCES TABLE

REAGENT or RESOURCE	SOURCE	IDENTIFIER
Other		
Commercial Ion exchange membrane	Versogen Inc.	Piperlon® 80 um
Commercial Ion exchange ionomer	Versogen Inc.	Piperlon® 5% dispersion
Custom Ion exchange membrane	Proprietary	50 um
Commercial Ion exchange ionomer	Proprietary	5% dispersion
Pt/HSC catalyst for hydrogen evolution reaction	Alfa Aesar	40% Pt supported on high surface carbon
Co_3O_4 catalyst for oxygen evolution reaction	US Research Nanomaterials Inc.	99%, 10–30 nm particle size
Stainless steel felt for anode	Bekaert	Currento® PTL SS-78/300
Nickel felt for anode	Bekaert	Currento® PTL Ni-60/250
Toray Carbon Paper for cathode	Toray	Toray Paper 90 - TGP-H-090
Ultrasonic bath for mixing inks	Fisher Scientific	FS30H
Potentiostat for electrochemical measurements	Autolab with 20 A booster	N/A
Catalyst loading measurements	Fisher Scientific	XRF- XDV-SDD

METHOD DETAILS

Detailed methods are provided in the online version of this paper and include the following:

Polymer membranes and ionomer

Two types of polymers are used in this study. One is a commercial PiperION (Versogen) anion exchange membrane (AEM) and ionomer purchased from Fuel Cell store. The films are 40 μm or 80 μm thick and ionomer dispersion (5 w%) is used for fabricating electrodes. The second polymer is a proprietary anion exchange membrane (AEM) polymer. The proprietary ionomer dispersion is prepared in-house (5 w%) using proprietary solvent composition and it does not undergo any heat treatment (used as is). For both commercial and homemade ionomers, the ionomer content in the ink is 30 w% for the anode and 25 w% for the cathode. The DIW/solvent ratio in the ink is 0.11. A schematic of film casting procedure using doctor blade and subsequent film drying process flow chart is presented in Figure S3. For this study the cast films are dried under three different conditions designated as, (a) *undried* (dried at 80°C for 0.5 hours only), (b) *dried at 60°C* (for 72 hours), and (c) *dried at 80°C* (for 72 hours). Following the drying process, the films are measured for dry thickness and recorded around 50 μm.

Ex-situ characterization of polymer films

For ex-situ characterizations, the AEM cast samples are first exchanged from bicarbonate $(HCO_3)^-$ to chloride $(Cl)^-$ form by soaking in 2.5 50M NaCl for 24 hours at room temperature. The material is then washed with DI water and dried in an oven at 60°C. Ion exchange capacity (IEC) is determined using the Mettler Toledo T90 auto titrator and a silver ring electrode to perform chloride titration using potentiometric indication. In this process, 50 mg of dry material is weighed and soaked in 1.0 M $NaNO_3$ overnight. This solution is then titrated using 0.1M $AgNO_3$ on the auto titrator until the equivalent point is reached. The IEC is then calculated from the weight of the sample and the amount of titrant required to reach the equivalence point.

Conductivity is measured using cells that hold a strip of membrane against four electrodes. The membrane is first soaked in DI water for 24 hours. Then the sample is cut into 5 mm wide strips and placed into the conductivity cell with a Styrofoam backing to keep the sample in contact with the electrodes. The cells are connected to the solartron analytical 1470E multi-channel potentiostat and are tested inside the Test Equity 1000 series temperature/humidity chamber. The resistance is measured at 60°C for relative humidity 95 % to 40 %. Using the resistance at each relative humidity, the conductivity is calculated. Dynamic water uptake is measured using TA Instruments TGA Q5000SA dynamic vapor sorption analyzer (DVS). First, 5mg of dry material is weighed and placed into a tared 100μL platinum pan. The pan is then moved into the humidity chamber where the temperature is controlled at 60°C as the relative humidity (%RH) changes from 0 % to 95 % and to 0 % again. The change in weight percent of the material at varying humidity yields the water uptake value.

Liquid water uptake measurements are performed by weighing dry film pieces and then soaking in deionized water for 24 hours. The weight change is used as the liquid water uptake. The following equation gives the liquid water uptake value, where W_w is the wet weight and W_d is the dry membrane weight.

$$\text{Water Uptake}\ (\%) = \frac{Ww - Wd}{Ww}$$

Electrode fabrication

The custom ionomer dispersion or 5 w% PiperIon dispersion ionomers is used to formulate catalyst inks by mixing deionized (DI) water and appropriate solvents. Cobalt-based electrocatalysts for oxygen evolution reaction (OER) while Pt-based electrocatalyst for hydrogen evolution reaction (HER) are used. 40% Pt/C (Alfa Aesar, Pt nominally 40 wt%, supported on carbon is used at the cathode for HER and Cobalt Oxide nano powder (Co_3O_4, 99 %, 10-30 nm, US Research Nanomaterials Inc.) are used at the anode for OER. The catalyst is added to a vial followed by DI water to wet the catalyst. Table 1 summarizes the electrode materials and loadings used in this study.

Next, ionomer dispersion is added to horn sonicate for 30 s. The mixture is then homogenized in an ultrasonic bath (Fisher Scientific FS30H) for 60 min while maintaining the bath temperature under 20°C. Then, the homogenized ink for cathode is sprayed onto Toray carbon GDLs 290 μm thick with 0% wet proofing. The ink for anode is sprayed onto Ni or stainless steel (SS) PTL 280 μm thick acquired from Bekaert. Both anode and cathode inks are airbrush sprayed directly onto the Ni, SS or carbon PTLs/GDLs. The PTLs/GDLs are mounted to a hot vacuum plate, 80°C while inks are sprayed layer by layer using Nitrogen flow through the airbrush. The deposition method has been adopted from our previous reports.[17,31] For all electrodes, inks are sprayed onto 25 cm^2 area substrates, which are then cut into smaller gas diffusion electrodes (GDEs) each with an active area of 5 cm^2. The noble metal loadings are measured using XRF Fisher XDV-SDD and desired loadings are achieved for the anode and cathode electrodes, 3.0±0.1 mg_{Co} cm^{-2}, and 0.25 ± 0.05 mg_{Pt} cm^{-2} respectively.

Membrane electrode assembly and testing

For *in situ* evaluation of the membrane's performance, the GDEs are formed into MEAs and loaded into a 25 cm^2 customized cell hardware (masked down to 5 cm^2) with a triple serpentine Nicke flow field plates and SS end plates. The first step in the MEA fabrication is to pretreat the AEMs and the GDEs to convert them to the OH^- form. This is done by soaking the membrane and electrodes in a 1.0 M KOH solution in separate containers for 48 h. Following pretreatment, the AEM is sandwiched between the anode and cathode GDEs (without any hot pressing) and the cell is torqued to 40 in. lb. using 10 mil PTFE sheet for anode and 11 mil for the cathode as the gasket materials. All the operating AEMWEs in this work are controlled using a customized electrolyzer single cell test station. At cell startup, DI water or 0.1 M or 1 M KOH is fed to both anode and cathode sides setting the electrolyte as well as cell temperature to 80°C. After reaching stable temperatures, the cell is connected to Autolab potentiostat with 20 A booster. The cell conditioning protocol employed here is discussed in the results section. For each AEM sample, cathodic (scanning from 2.0, 1.9, 1.8, 1.7, 1.65, 1,6, 1.55, 1.53, 1.48, 1.46, 1.44, 1.42, 1.41 and 1.40 V descending order) and anodic (scanning from 1.40 V to 2.0 V in ascending order) polarization data are recorded. Only anodic scans are presented as polarization curves for all experiments. The electrochemical impedance spectra (EIS) are collected at 1.4, 1.41, 1.42, 1.44, 1.46, 1.48, 1.5, 1.55, 1.6, 1.65, 1.7, 1.8, 1.9 and 2.0 V. The cyclic voltammograms (CVs) are recorded at 100 mV/s scan rate. Durability evaluations at constant current hold are done followed by collecting end of test polarization plots, EIS and CVs for degradation analysis.

QUANTIFICATION AND STATISTICAL ANALYSIS

None.